NACA

RESEARCH MEMORANDUM

INVESTIGATION AT ZERO ANGLE OF ATTACK OF A 16-INCH

RAM-JET ENGINE IN 8- BY 6-FOOT SUPERSONIC
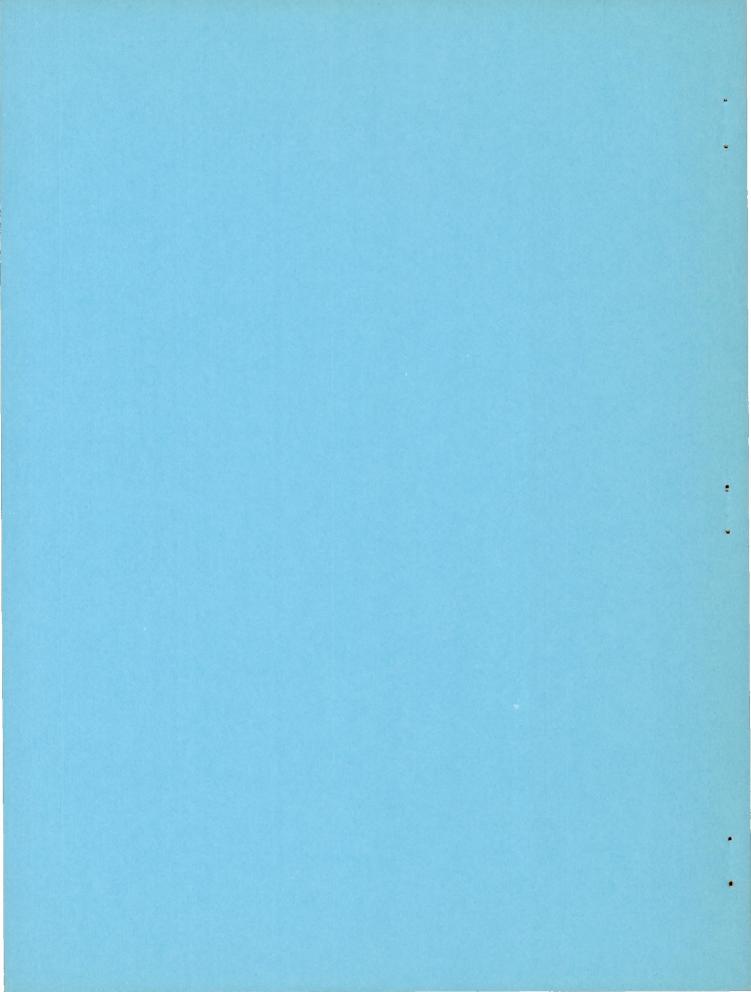
WIND TUNNEL

By T. Nussdorfer, F. Wilcox, and E. Perchonok

Lewis Flight Propulsion Laboratory
Cleveland, Ohio

NATIONAL ADVISORY COMMITTEE
FOR AERONAUTICS

WASHINGTON

March 2, 1951
Declassified December 3, 1958

NATIONAL ADVISORY COMMITTEE FOR AERONAUTICS

<u>RESEARCH MEMORANDUM</u>

INVESTIGATION AT ZERO ANGLE OF ATTACK OF A 16-INCH RAM-JET ENGINE

IN 8- BY 6-FOOT SUPERSONIC WIND TUNNEL

By T. Nussdorfer, F. Wilcox, and E. Perchonok

SUMMARY

A study was made in the NACA Lewis 8- by 6-foot supersonic wind tunnel of the performance of a 16-inch ram-jet engine at zero angle of attack and over a range of free-stream Mach numbers between 1.5 and 2.0. The engine was equipped with a single-oblique-shock 50° cone inlet and a cylindrical constant-area exit nozzle. The study was made with a can-type flame holder using propylene oxide as fuel.

Maximum propulsive thrust coefficients in the order of 0.55 and net internal thrust coefficients of 0.725 were obtained at Mach numbers 1.5, 1.8, and 2.0. No special combustion or operational problems were encountered over a range of burner-inlet Mach numbers from 0.220 to 0.367 and total-temperature ratios between 2.0 and 5.5.

Reasonable agreement was noted between the experimentally determined additive and cowl pressure drags and the theoretically predicted values.

Some subcritical diffuser instability was encountered at Mach numbers of 1.8 and 2.0.

INTRODUCTION

As part of a general program to study and evaluate the ram jet as a supersonic power plant, an experimental investigation of the performance of a typical 16-inch ram-jet engine was undertaken in the NACA Lewis 8- by 6-foot supersonic wind tunnel. The engine was designed for a flight Mach number of 1.8 and had a single-oblique-shock external-compression inlet. Engine performance was investigated at six free-stream Mach numbers between 1.5 and 2.0 and at angles of attack from 0° to 10°. The Reynolds number, based on diffuser-inlet diameter, varied from 4.56×10^6 to 4.92×10^6. Based on engine length, the Reynolds number varied from 77.5×10^6 to 81.1×10^6.

Specific objectives of the investigation were (1) to evaluate the net performance of the engine; (2) to compare the measured drag of a burning ram-jet engine with values calculated from small-scale cold-flow investigations and with existing theories; and (3) to investigate the effect of changes in flight Mach number and fuel-air ratio on diffuser and combustion-chamber stability

This report presents an evaluation at zero angle of attack of total and component engine body drags, internal engine performance, and the net propulsive thrust developed by this engine with a cylindrical constant-area exit nozzle.

APPARATUS

The installation of the ram-jet engine in the 8- by 6-foot supersonic wind tunnel is shown schematically in figure 1. A sweptback vertical strut attached to the tunnel balance frame supported the engine. The inlet was located in the region of the test-section windows and a schlieren system was employed to study the shock formation about the diffuser inlet.

The engine consisted of a diffuser 9.34 feet long and a combustion chamber and nozzle 6.25 feet long (fig. 2). The supersonic diffuser was so designed that the oblique shock generated by the 25° half-angle conical spike would fall slightly ahead of the cowl lip at a free-stream Mach number of 1.8. Internal and external dimensions of the engine are given in table I. The diffuser and the center body were constructed of steel and the combustion chamber and the exit nozzle were made of 1/8-inch Inconel.

A vortex pilot similar to that described in reference 1 was employed. A blend by volume of 50-percent gasoline and 50-percent propylene oxide was used as a pilot fuel and was introduced through a commercial spray nozzle rated at 12.5 gallons per hour at a differential pressure of 100 pounds per square inch.

The can-type flame holder (references 2 and 3) had a surface open area of 133 percent of the combustion-chamber frontal area. The fuel system consisted of two independently controlled manifolds having commercial nozzles spraying fuel within the flame holder. A diagram of the flame holder and the fuel-nozzle arrangement is shown in figure 3. In order to obtain smooth pulsation-free combustion, it was found necessary to use propylene oxide as fuel.

Details of static- and total-pressure surveys at stations 2 and x are indicated in figure 4. A water-cooled total-pressure rake, which was not attached to the tunnel scales, was located at the combustion-chamber exit to obtain internal engine performance. Static wall orifices were located on the forward section of the outer shell of the diffuser and along the diffuser inner wall and center body. Fluctuations in pressure at station 2 were determined with a commercial differential-pressure pickup.

The total temperature and pressure level in the test section depended on the Mach number and the atmospheric conditions and could not be controlled.

PROCEDURE

A cold-flow investigation to establish the effect of mass flow and combustion-chamber-inlet Mach number on diffuser recovery and external drag preceded the investigation with combustion. A remotely adjustable valve was installed at the flame-holder station to control the combustion-chamber inlet Mach number over both the subcritical and supercritical flow range.

The mass flow was computed from the data obtained at station x (fig. 2). The instrumentation at this station was calibrated by correlation with air-flow measurements at station 2, with data from a 1/2-scale version of this inlet, with mass flows determined from measurements of shock structure on schlieren photographs (reference 4), and with maximum capture area flows for the supercritical case. The air mass flow is believed to be accurate within ±3 percent.

The total pressure at the combustion-chamber inlet (station 3) was found to be the same (within the accuracy of the measurement) as that at station x. Accordingly, the diffuser pressure recovery is expressed in terms of a total pressure at station x calculated from the mass flow and the measured static pressure. Burner-inlet Mach numbers are based on the annular area at the diffuser exit.

In order to separate the engine body drag from the support strut drag, additional runs were made with a dummy strut identical in every way with the support strut. The technique of using a dummy strut to evaluate support strut drag is discussed in reference 5. In general, the assumptions required are that the strut drag and the body-strut interference drags are double the values for the case with the support strut alone. A photograph of the installation showing the engine, the support strut, and the dummy strut is shown in figure 5.

Without combustion, the static pressure and area at the nozzle exit and the air mass flow were used in obtaining jet thrust. With combustion the nozzle exit was assumed choked and the jet thrust computed from tail-rake total-pressure data. Combustion efficiency and gas total-temperature rise were computed by the methods generally employed and outlined in references 6 and 7. The heat lost to the air stream in cooling the combustion chamber could not be included in the evaluation of the combustion efficiency and the gas total-temperature rise. The combustion efficiency is defined as the ratio of the change in energy of the gases flowing through the engine to the lower heating value of the fuel being injected.

Most of the data are conveniently expressed as a function of the mass-flow ratio m/m_0. This parameter is defined as the ratio of the actual air mass flow through the engine to the mass flow contained in a free-stream tube having a diameter equal to the diffuser-inlet diameter.

SYMBOLS

The following symbols are used in this report:

A   area, (sq ft)

C   force coefficient, $F/q_0 A_{max}$

F   force, (lb)

f/a   fuel-air ratio

h   lower heating value of fuel, (13,075 Btu/lb for propylene oxide)

J   mechanical equivalent of heat, (778 ft-lb/Btu)

M   Mach number

m   mass flow, (slugs/sec)

P   total pressure, (lb/sq ft absolute)

p   static pressure, (lb/sq ft absolute)

q   dynamic pressure, $\frac{\gamma}{2} pM^2$

T   total temperature, $^\circ R$

V   velocity, (ft/sec)

W_f fuel flow, (lb/sec)

$\dfrac{(F_t-F_d)V_0}{\eta_b h W_f J}$ engine efficiency (reduced to 100-percent combustion efficiency)

γ ratio of specific heats

η_b combustion efficiency

τ total-temperature ratio across engine

Subscripts:

a   additive drag

d   total body drag

f   friction drag

max   maximum

p   pressure drag

t   thrust

x   air-flow measuring station (59 in. from cowl lip)

0   free stream

1   engine inlet

2   alternate air-flow measuring station (18 in. from cowl lip)

3   combustion-chamber inlet

4   nozzle inlet

6   nozzle exit

RESULTS AND DISCUSSION

Diffuser Performance

The variation of the combined subsonic and supersonic total-pressure recovery across the diffuser P_x/P_0 and mass-flow ratio m/m_0

with combustion-chamber-inlet Mach number M_3 is presented in figure 6 at free-stream Mach numbers M_0 of 1.5, 1.8, and 2.0 for both cold-flow and burning conditions. It is noted that for this particular diffuser configuration the critical mass flow occurred at M_3 of approximately 0.195 at all three flight Mach numbers. At M_0 of 1.5 the pressure recovery was close to the normal shock recovery over the entire sub-critical range investigated. Although peak pressure recoveries considerably above normal shock recovery were observed at M_0 of 1.8 and 2.0, a rather sharp drop in pressure recovery was observed at a Mach number of 2.0 as the flow was reduced below the critical value. Maximum mass-flow ratios of 0.776, 0.920, and 1.000 resulted at Mach numbers of 1.5, 1.8, and 2.0, respectively. Because of the large nozzle-outlet area, no combustion data could be obtained in the subcritical region of any of the Mach numbers investigated.

Representative schlieren photographs of the points labeled A, B, C, and D on figure 6 are shown in figure 7. A small amount of contraction in the first 1/2 inch of the inlet prevented the normal shock from entering the inlet at Mach numbers below 2.0. (Compare A and B, fig. 7).

Shock pulsations were observed in the subcritical flow range at Mach numbers of 1.8 and 2.0. Such pulsations are undesirable not only because they reduce the diffuser total-pressure recovery, but because they can also cause burner instability and blow-out. In order to illustrate the magnitude of these pulsations, traces of the static-pressure fluctuations at station 2 for conditions C and D are shown in figure 7. At peak pressure recovery (fig. 7(c)), a slight amount of normal shock movement can be observed. Considerably more movement is evident when the mass-flow ratio is reduced (fig. 7(d)). The frequency and the magnitude of static-pressure fluctuation at station 2 under critical-flow conditions (fig. 7(c)) were 4.5 cycles per second and plus 4.5 percent of a base pressure, respectively. The instantaneous pressure record indicates that the fluctuation was in the form of small pressure surges above the base value. The instantaneous pressure record for point D indicates a frequency of 17.9 cycles per second and the fluctuation of ±17.4 percent of the average pressure. From the schlieren photographs for this condition, the normal shock appears to travel from the lip out to a point two-thirds the length of the spike.

Drag Evaluation

Drag characteristics of the configuration were investigated under cold-flow conditions over a range of mass-flow ratios. Under burning conditions, the drag characteristics could be investigated only at the

maximum mass-flow ratio at each Mach number. No measurable difference could be found in the total body drag between cold flow and burning conditions. It was also determined that, within the accuracy of the data, the interference drag between struts or of the strut on the body was negligible.

Variation with M_0 of the total body drag coefficient (as determined by force measurements) for a range of mass-flow ratios is shown in figure 8. The dashed lines representing the minimum drag coefficient indicate the same general trend for this ram-jet configuration and for an 8-inch configuration of similar external geometry but having a lower combustion-chamber length to diameter ratio. The minimum drag coefficient decreased linearly from 0.2 at $M_0 = 1.5$ to 0.163 at $M_0 = 2.0$ (fig. 8). At a given Mach number the drag increased rapidly with decreasing mass flow.

The theoretical additive drags (all component and body drag coefficients are based on the combustion-chamber area A_{max}) calculated by a method similar to that described in reference 8 are compared in figure 9 with the experimentally determined values calculated from a momentum balance between stations 0 and 1. Results are presented in terms of mass-flow ratio for M_0 of 1.5, 1.8, and 2.0. In general, at a given M_0 the experimental additive drag decreased linearly as the mass-flow ratio increased. Considering the assumptions made in deriving the theoretical curves and that the effect of friction has been neglected in the experimental evaluation of additive drag, the excellent agreement between simple theory and experimental data is probably coincidental.

Component drag coefficients at M_0 of 1.5, 1.8, and 2.0 are summarized in figure 10 and compared with total body drags derived from the scale measurements and indicated in figure 8. The cowl pressure drag coefficients, which were obtained by graphical integration of the pressure coefficients along the cowl surface, increased linearly with mass-flow ratio. It is of interest that where data were available at the same mass-flow ratio for all three Mach numbers, essentially identical cowl drag coefficients were recorded. Moreover, below a mass-flow ratio of approximately 0.6, leading-edge suction on the external cowl surface results in a positive thrust force. The experimentally determined cowl pressure drag for a mass flow ratio of 1 at $M_0 = 2.0$, (fig. 10(c)) agreed reasonably well with the value computed from linearized potential theory (the local pressure coefficient taken equal to $-2\frac{V_x}{U_0}$, where V_x is the local perturbation velocity in the direction of the engine axis and U_0 is the flight velocity). These results are consistent with data obtained during studies of an 8-inch-diameter diffuser (reference 9).

Friction drag was not measured; however, theoretical values were obtained from coefficients based on turbulent compressible flow over a smooth flat plate (reference 10). (This procedure yielded agreement with experimentally determined friction coefficients for an 8-inch diameter body having the same general shape as this engine, reference 11). At a given M_0, the calculated friction drag coefficients were assumed constant for all mass-flow ratios and were based on test-section conditions, wetted body surface area, and a Reynolds number based on a total body length.

Comparison of the summation of the drag components with the total drag obtained from the scales (fig. 10) indicates varying degrees of agreement. The cause of these discrepancies is not known, but may arise from inadequacies in evaluating either the measured total engine drag or any of the component drags. Among the latter, error in the estimated friction drag is more likely than in the additive or cowl pressure drags.

Engine Evaluation

The experimental variation of the net-thrust coefficient C_t with the total-temperature ratio across the engine τ is shown in figure 11. An improvement in cycle efficiency with increasing M_0 resulted in essentially the same maximum net-thrust coefficient 0.725 for all three free-stream Mach numbers in spite of a decrease in the maximum τ as M_0 was raised.

These net-thrust-coefficient data are characteristic of the particular internal engine configuration investigated. Such data can be combined with the external drag of the body in which the engine will be used to determine the propulsive thrust that will be developed. For this engine the experimental internal-thrust data of figure 11 (supercritical conditions) have been combined with the minimum-drag data of figure 8 to indicate the net propulsive thrust developed. Because identical supercritical drags were determined for this configuration under both cold-flow and burning conditions, this procedure is considered valid for critical mass flows.

The variation in engine thrust minus drag (or propulsive thrust coefficient) with flight Mach number for a range of τ is indicated in figure 12 as cross plots of experimental data. These data show that the propulsive thrust coefficient increased with M_0 for a given τ and that a fixed propulsive thrust coefficient can be maintained as the Mach number is raised by reducing τ. For example, at M_0 of 2.0

a body thrust minus drag coefficient of 0.55 was obtained with a τ of 4.25, whereas at an M_O of 1.5 a τ of 5.6 would be required to deliver the same propulsive thrust.

The efficiency of this engine as a propulsive device is indicated in figure 13. The parameter has been idealized to 100-percent combustion efficiency and in its present form can be applied to this engine for any fuel and any combustion efficiency. Because it is small, the kinetic energy of the fuel at injection has been neglected. Corresponding values of M_3 and τ are included in figure 13 for convenience in interpretation. Engine thrust must exceed the engine body drag to result in a positive engine efficiency. With this particular configuration, a positive engine efficiency occurred at τ greater than 2.0 for a Mach number of 2.0 and would occur at slightly higher values of τ at lower Mach numbers.

Operation of a fixed-geometry engine at design conditions does not necessarily imply that the peak over-all engine efficiency occurs simultaneously with maximum τ or maximum thrust minus drag. For off-design supercritical operation, however, such as is the case with this configuration, raising τ does cause increases in both engine efficiency and $(C_t - C_d)$. The trends obtained indicate that increases in τ beyond the maximum experimental values to achieve operation at the critical or design condition will result in greater thrust minus drag values but will cause little gain in engine efficiency. Further increases in τ will result in subcritical operation and ultimate reduction in engine efficiency.

The effect of an increase in Mach number M_O was a marked increase in the engine-efficiency parameter. A maximum value of nearly 0.15 was obtained at $M_O = 2.0$.

Burner Performance

Burner-performance data are presented in figure 14. Complete burner evaluation was not undertaken because it was not necessary to the primary objective of the investigation. It was only necessary to develop a burner having satisfactory operational characteristics over a range of Mach numbers from 1.5 to 2.0 and at angles of attack up to 10°. Such operation was achieved with a can-type flame holder and with propylene oxide as fuel. The variation with fuel-air ratio of combustion efficiency η_b, ratio of total temperature at combustion-chamber exit to total temperature at combustion-chamber inlet τ, and

combustion-chamber-inlet Mach number M_3 is shown for three free-stream Mach numbers. Great significance should not be attached to the variation of burner performance with flight Mach number because the proportion of fuel to the primary and secondary fuel manifolds was not the same for all three values of M_0 and at all fuel-air ratios. Neither lean nor rich blow-out limits were encountered. The maximum fuel-air ratio was limited by the capacity of the fuel-handling system.

Burning occurred at values of M_3 ranging from 0.220 to 0.367 and over a range of f/a from 0.029 to 0.081 (stoichiometric f/a for propylene oxide is 0.105). The maximum τ decreased from 5.50 at M_0 of 1.5 to 4.25 at M_0 of 2.0. Absolute values of combustion efficiency and τ are probably no more accurate than ±5 percent, because an error of 3 percent in the air flow in the lean fuel-air ratio region would result in a 5-percent change in combustion efficiency.

SUMMARY OF RESULTS

The performance of a typical 16-inch ram-jet engine was investigated in the 8- by 6-foot supersonic wind tunnel at an angle of attack of 0° and at Mach numbers from 1.5 to 2.0. The engine was equipped with a single-oblique-shock 50° spike diffuser and a cylindrical constant-area exit nozzle. The following results were obtained:

1. At a free-stream Mach number of 2.0, a total-temperature ratio across the engine in excess of 2.0 was required for propulsive thrust to be delivered by the engine. Maximum propulsive thrust coefficients in the order of 0.55 and maximum net internal thrust coefficients of 0.725 were obtained at Mach numbers of 1.5, 1.8, and 2.0.

2. Comparison of the summation of the drag components with the total engine drag obtained from the scales indicates varying degrees of agreement.

3. The cowl pressure drags increased linearly with mass-flow ratio and at a given mass-flow ratio were negligibly affected by variation in Mach number from 1.5 to 2.0. Agreement was noted between the experimental data and the value theoretically predicted for a mass-flow ratio of 1 at Mach number 2.0.

4. The additive drag increased approximately linearly as the mass-flow ratio decreased. Reasonable agreement was noted between the experimental data and the additive drag predicted from one-dimensional theory.

5. The burner operated over a range of inlet Mach numbers from 0.220 to 0.367 and a range of total-temperature ratio across engine between 2.0 and 5.5.

6. Under-cold flow conditions, some subcritical diffuser instability was encountered at free-stream Mach numbers 1.8 and 2.0. Due to the large exit-nozzle area, however, the engine could not be operated subcritically with burning, and the effect of the diffuser instability on burner performance could not be established.

Lewis Flight Proplulsion Laboratory,
    National Advisory Committee for Aeronautics,
        Cleveland, Ohio.

REFERENCES
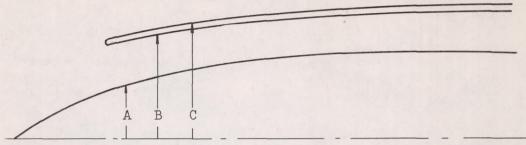
1. Nussdorfer, T. J., Sederstrom, D. C., and Perchonok, E.: Investigation of Combustion in 16-Inch Ram Jet under Simulated Conditions of High Altitude and High Mach Number. NACA RM E50D04, 1950.

2. Dupree, D. T., Nussdorfer, T. J., and Sterbentz, W. H.: Altitude-Wind-Tunnel Investigation of Various Can-Type Burners in Bumblebee 18-Inch Ram Jet. NACA RM E8L20, 1949.

3. Dailey, C. L., McFarland, H. W., and DeVault, R. T.: Development of Ramjet Components. Prog. Rep. 9961-4, Univ. Southern Calif. Aero. Lab., USCLA, June 7, 1949. (Bi-Monthly Prog. Rep. April-May 1949 under Navy Contract NOa(s)9961.)

4. Moeckel, W. E.: Approximate Method for Predicting Form and Location of Detached Shock Waves Ahead of Plane or Axially Symmetric Bodies. NACA TN 1921, 1949.

5. Mattson, Axel T.: Force and Longitudinal Control Characteristics of a 1/16-Scale Model of the Bell XS-1 Transonic Research Airplane at High Mach Numbers. NACA RM L7A03, 1947.

6. Perchonok, Eugene, Wilcox, Fred A., and Sterbentz, William H.: Preliminary Development and Performance Investigation of a 20-Inch Steady-Flow Ram Jet. NACA ACR E6D05, 1946.

7. Perchonok, Eugene, Sterbentz, William H., and Wilcox, Fred A.: Performance of a 20-Inch Steady-Flow Ram Jet at High Altitudes and Ram-Pressure Ratios. NACA RM E6L06, 1947.

8. Dailey, C. L., and McFarland, H. W.: Development of Ramjet Com-
   ponents. Prog. Rep. 9961-8, Univ. Southern Calif. Aero. Lab.,
   USCLA, Feb. 7, 1950. (Bi-Monthly Prog. Rep. Dec. 1949-Jan. 1950
   under Navy Contract NOa(s)9961.)

9. Esenwein, Fred T., and Valerino, Alfred S.: Force and Pressure
   Characteristics for a Series of Nose Inlets at Mach Numbers from
   1.59 to 1.99. I - Conical Spike All-External Compression Inlet
   with Subsonic Cowl Lip. NACA RM E50J26, 1951.

10. de Kármán, Th.: The Problem of Resistance in Compressible Fluids.
    Quinto Convegno "Volta", Reale Accademia d'Italia (Roma),
    Sett. 30-Ott. 6, 1935, pp. 3-57.

11. Luidens, Roger W., and Madden, Robert T.: Interpretation of
    Boundary-Layer Pressure-Rake Data in Flow with a Detached Shock.
    NACA RM E50I29a, 1950.

2064

TABLE I - 16-INCH RAM-JET COORDINATES

Station (in.)	Location	A	B	C	Miscellaneous
-5.05	Tip of spike	0			
-4.0		0.48			
-3.0		0.94			
-2.0		1.41			
-1.0		1.88			
0	Lip of inlet	2.34	5.05		Lip radius 0.032
1.0		2.78	5.13	5.37	
2.0		3.10	5.30	5.54	
3.0		3.36	5.45	5.69	
4.0		3.58	5.59	5.83	
6.0		3.94	5.83	6.07	
8.0		4.21	6.03	6.28	
10.0		4.40	6.20	6.45	
12.0		4.52	6.36	6.61	
14.0		4.58	6.48	6.72	
16.0		4.60	6.58	6.82	
18.0	Station 2	4.58	6.61	6.85	
30.0		4.44	Straight	Straight	
46.0		4.02	taper	taper	
59.0	Station x	3.08	7.75	8.13	
63.0		2.43	7.45	Cylindrical	
68.4	End of center body	0	7.38	section	
81	Pilot air inlets	1.5			
93	Pilot maximum diameter	4.0			
107	Station 3	3.3	8.00		
187	Nozzle exit		8.00	8.13	
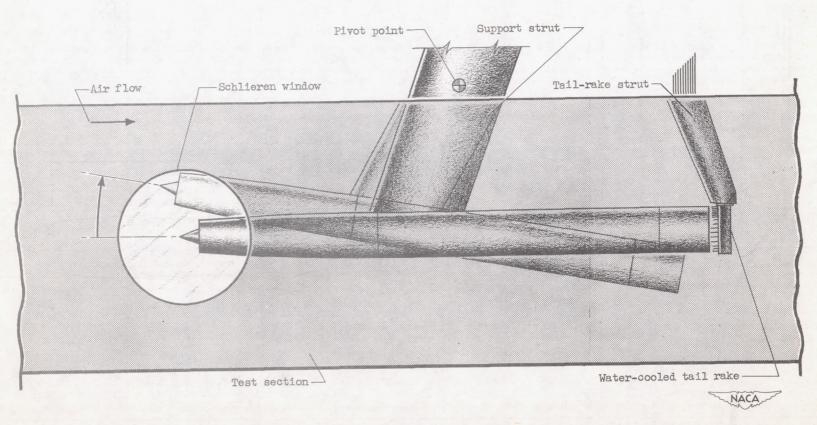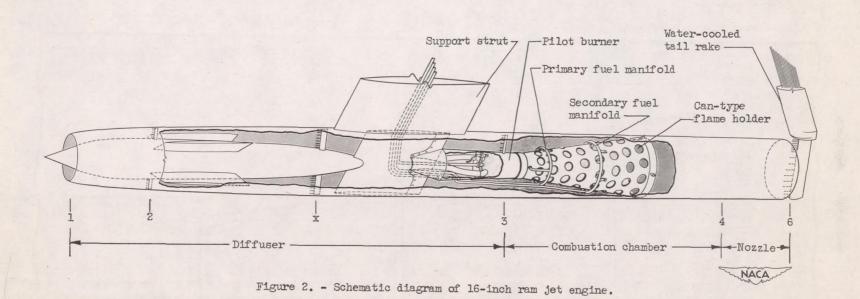
Figure 1. - Schematic diagram of installation of 16-inch ram-jet engine in 8- by 6-foot supersonic tunnel.

Figure 2. - Schematic diagram of 16-inch ram jet engine.

Single conical
nozzle directed
radially inward
0.358 gal 1 min

36"

$6\frac{3}{8}$"

$14\frac{3}{8}$"

Secondary
fuel manifold

Primary
fuel manifold

Nozzle arrangement at
primary manifold

Nozzle arrangement at
secondary manifold

Nozzle spray	Spray direction	Nozzle rating (at 100 lb/sq in.) (gallons/min)	
		Primary manifold	Secondary manifold
○ Conical	Radial		
□ Conical	45° upstream	0.667	1.000
◇ Conical	45° downstream		
△ Flat	Downstream	.625	.625

Figure 3. - Burner-configuration details.

Trailing edge of
center body support
struts located in
this position but
13 inches upstream
of this station

Station x

○ Total pressure
□ Static pressure

Station 2
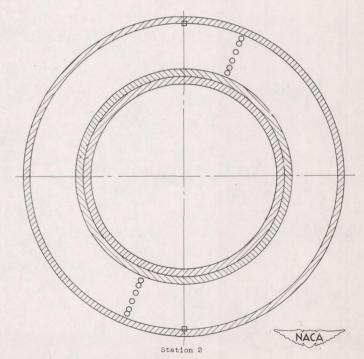
Figure 4. - Air-flow instrumentation details.
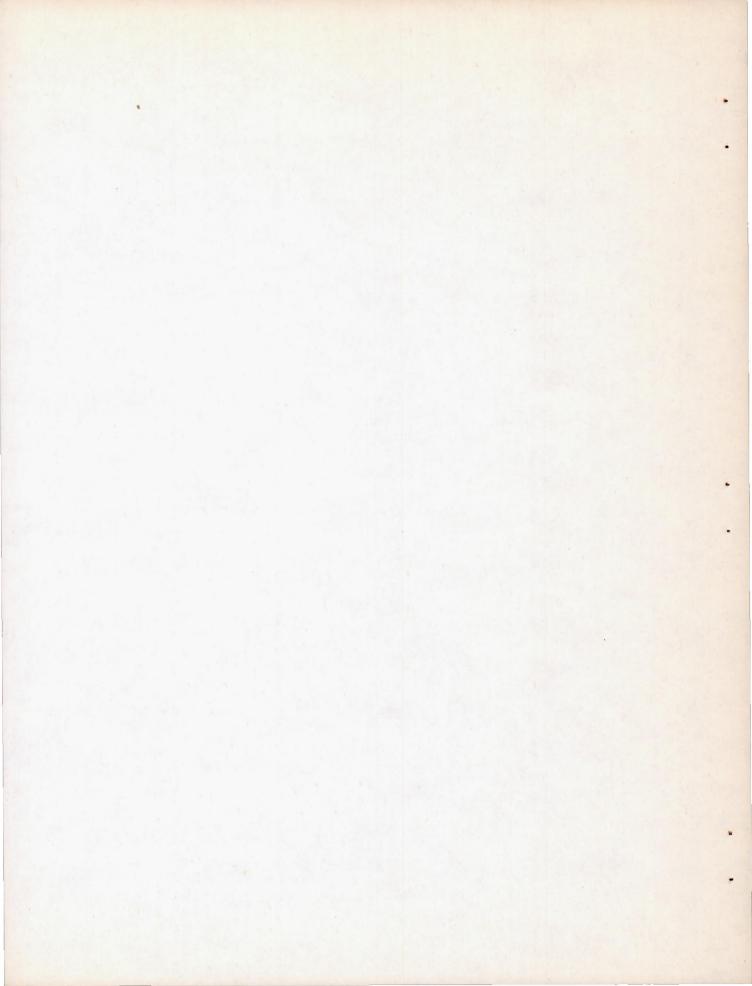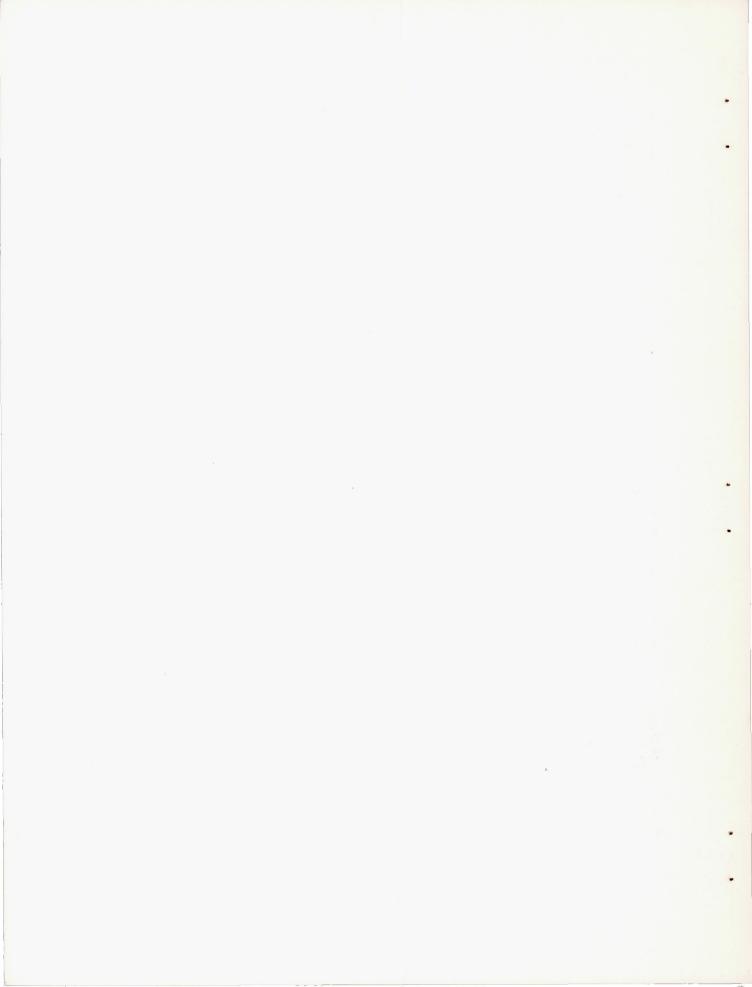
Figure 5. - Installation of 16-inch ram-jet engine in test section of 8- by 6-foot supersonic tunnel with dummy strut.
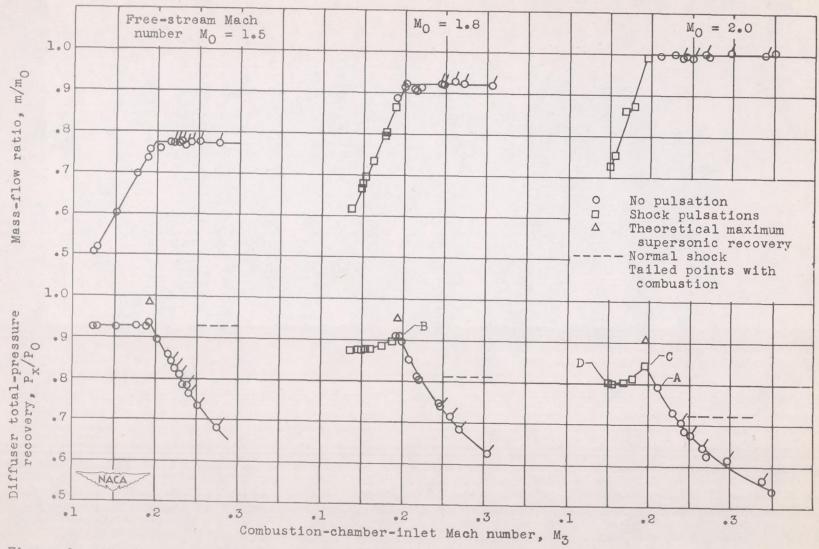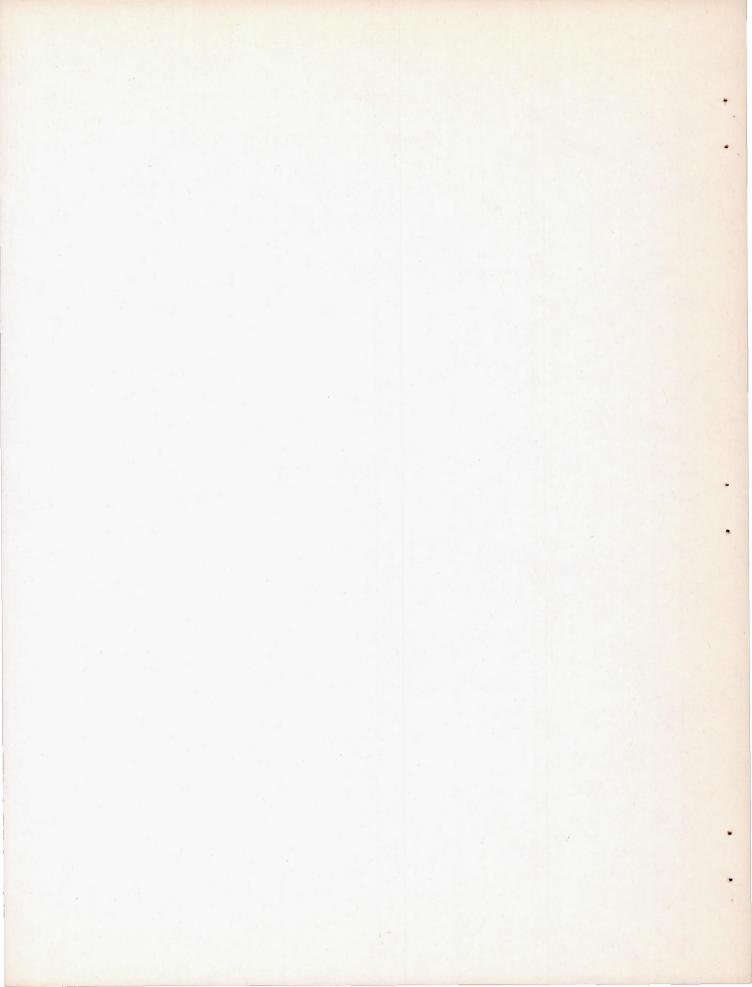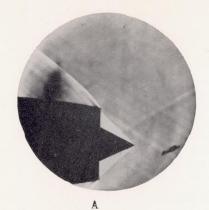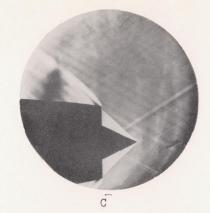
Figure 6. - Variation of diffuser total-pressure recovery and mass-flow ratio with combustion-chamber-inlet Mach number.

A

$M_O = 2.0$; $m/m_O = 1$

C
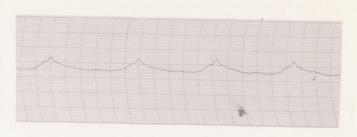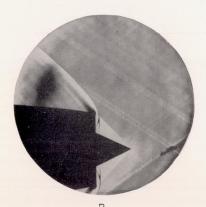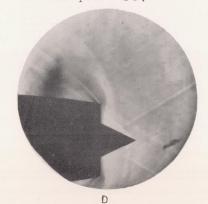
$M_O = 2.0$; $m/m_O = 0.995$;
frequency, 4.5 cycles per
second; $\Delta p = 115$ pounds per
square foot (+4.5 percent
of base pressure)

Pressure trace for C

B

$M_O = 1.8$; $m/m_O = 0.92$

D
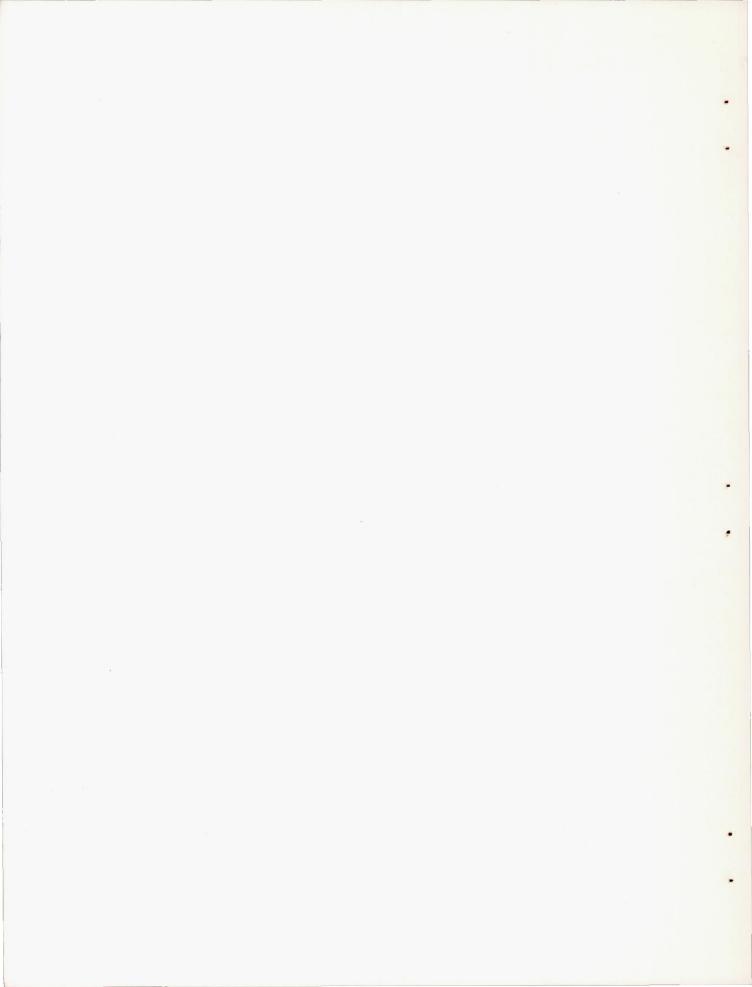
$M_O = 2.0$; $m/m_O = 0.733$;
frequency, 17.9 cycles per
second; $\Delta p = \pm461$ pounds per
square foot (±17.4 percent
of average pressure)

Pressure trace for D

NACA
C-26794

Figure 7. — Representative schlieren photographs and pressure traces.
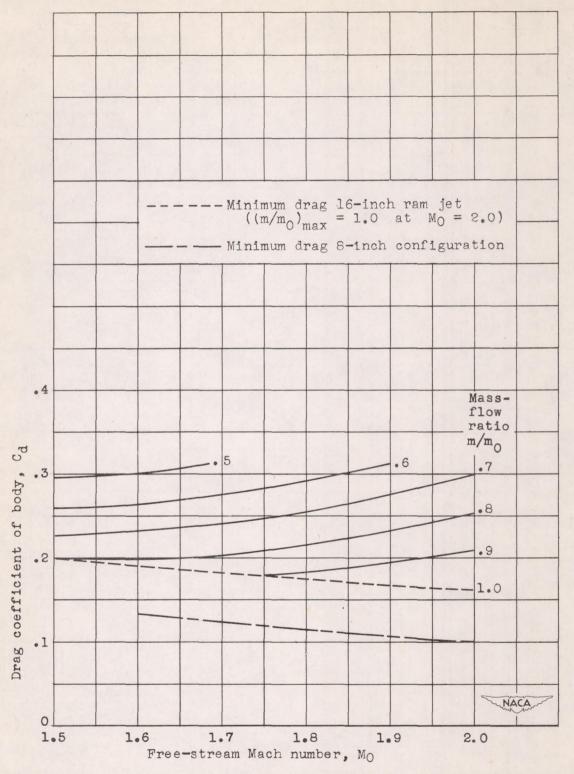
Figure 8. - Effect of free-stream Mach number and mass-flow ratio on engine body drag coefficient obtained from force measurements.
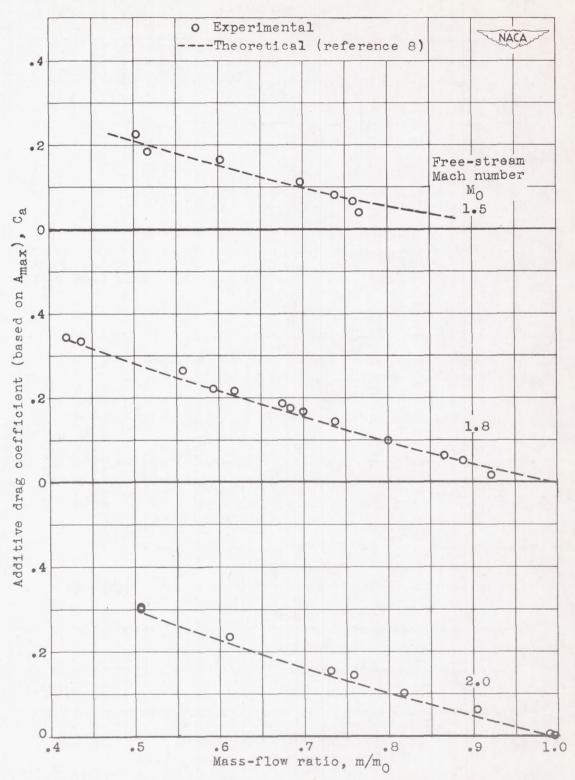
Figure 9. - Effect of mass-flow ratio on experimental and theoretical additive drag.

(a) Free-stream Mach number, 1.5.

(b) Free-stream Mach number, 1.8.
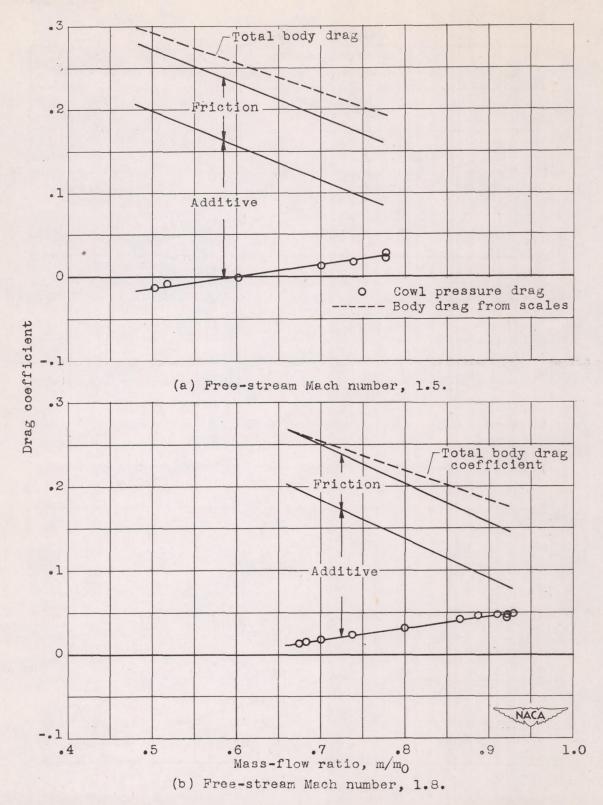
Figure 10. - Variation of component drag coefficients with mass-flow ratio.

(c) Free-stream Mach number, 2.0.
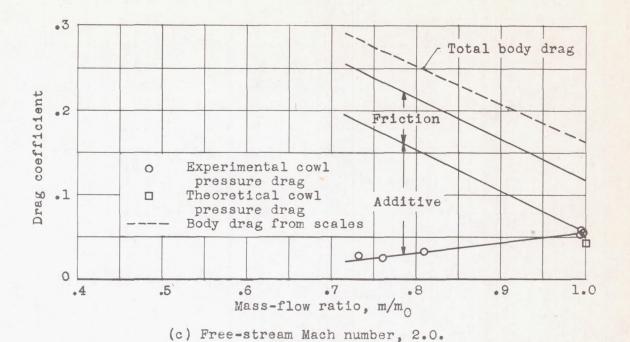
Figure 10. - Concluded. Variation of component drag coefficients
with mass-flow ratio.
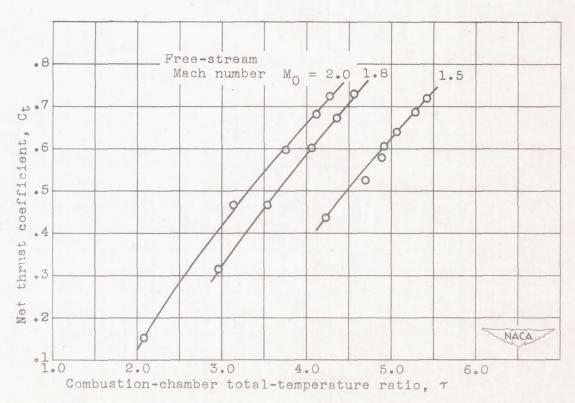
Figure 11. - Variation of net thrust coefficient with gas total-
temperature ratio.
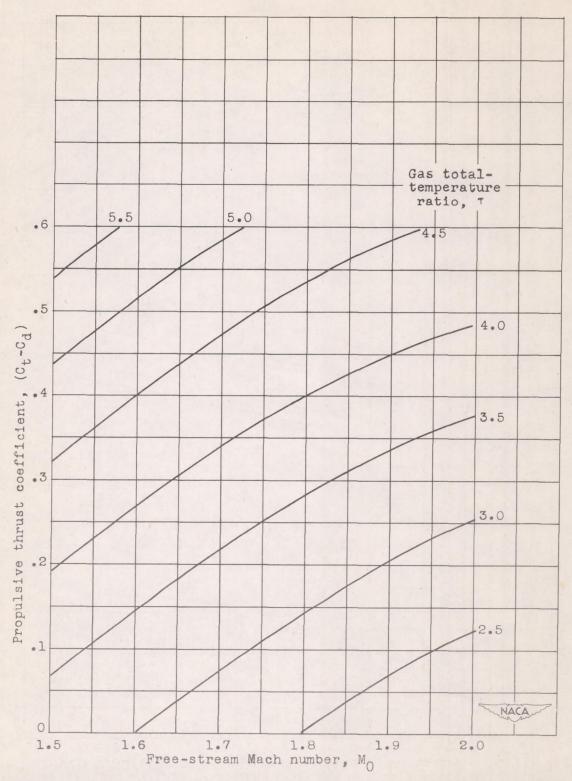
Figure 12. – Variation of propulsive thrust coefficient with free-
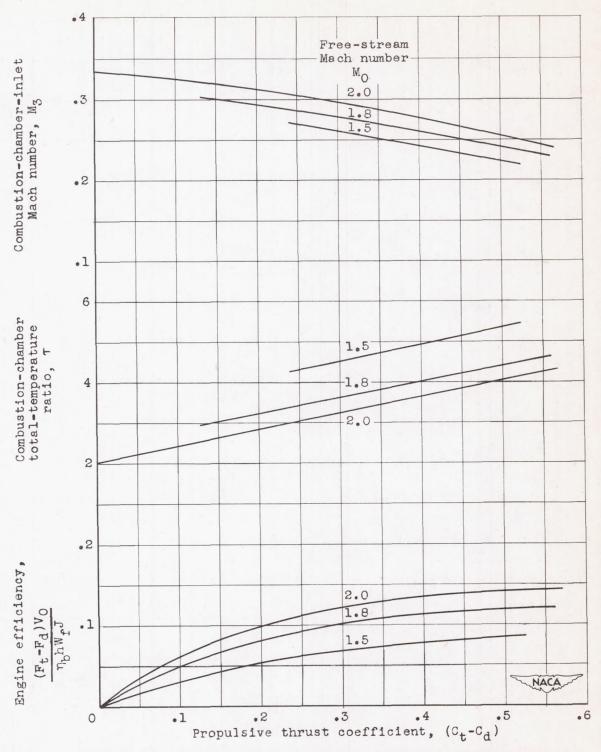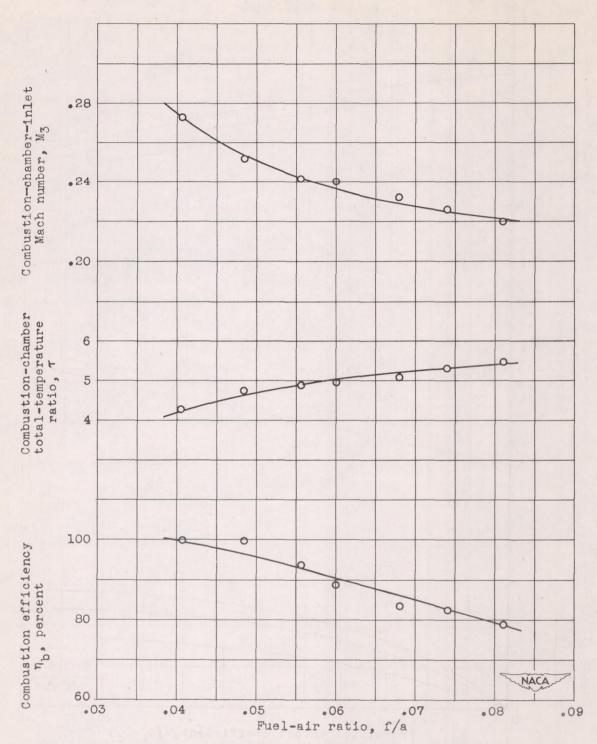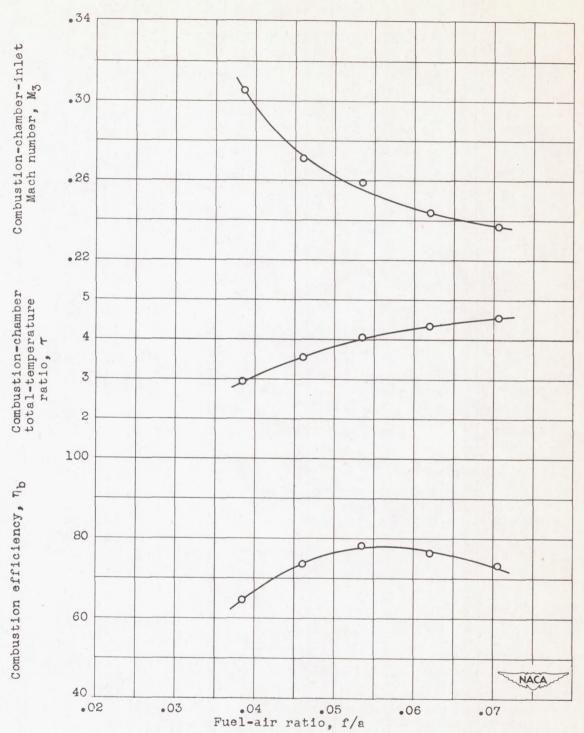stream Mach number and gas total-temperature ratio.

Figure 13. – Variation of engine efficiency, gas total-temperature ratio, and combustion-chamber-inlet Mach number with propulsive thrust coefficient.
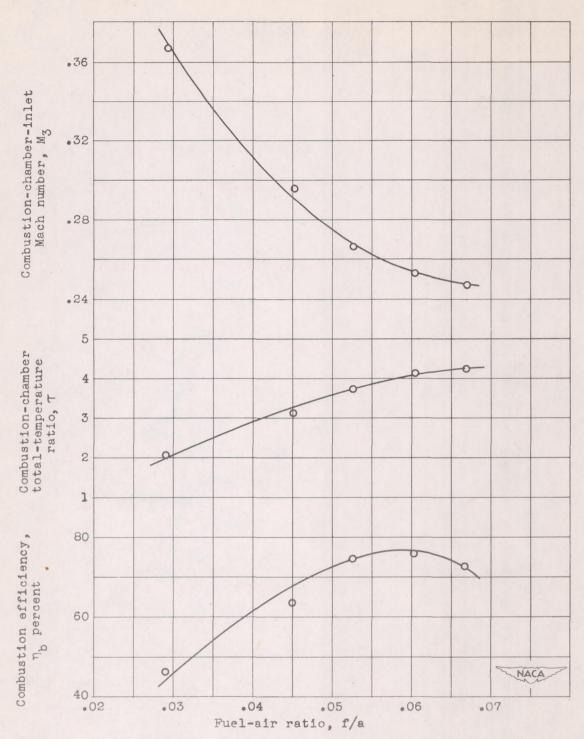
(a) Free-stream Mach number, 1.5; pressure altitude, 28,000 feet;
combustion-chamber-inlet temperature, 110° F.

Figure 14. - Effect of fuel-air ratio on combustion efficiency, gas
total-temperature ratio, and combustion-chamber-inlet Mach number.

NACA RM E50L04

(b) Free-stream Mach number, 1.8; pressure altitude, 34,000 feet; combustion-chamber-inlet temperature, 136° F.

Figure 14. - Continued. Effect of fuel-air ratio on combustion efficiency, gas total-temperature ratio, and combustion-chamber-inlet Mach number.

(c) Free-stream Mach number, 2.0; pressure altitude, 37,000 feet; combustion-chamber-inlet temperature, 157° F.

Figure 14. - Concluded. Effect of fuel-air ratio on combustion efficiency, gas total-temperature ratio, and combustion-chamber-inlet Mach number.